Validation of the 4C Code on the AC Loss Tests of a Full-Scale ITER Coil

Validation of the 4C Code on the AC Loss Tests of a Full-Scale ITER Coil

A. Zappatore, R. Bonifetto, *Member, IEEE*, N. Martovetsky, and R. Zanino, *Senior Member, IEEE*

***Abstract*—The AC loss tests on the first ITER Central Solenoid Module (CSM) have been modelled and compared to the test results. The model has been implemented in the 4C code, a thermal-hydraulic modelling tool which includes the CSM winding pack and the cryogenic circuit of the test facility. Two modes of operation of the circuit have been analyzed: the nominal and the "isolation" mode, i.e., when the cryogenic circuit valves are operated to isolate the coil during the current dumps. The computed mass flow rate, pressure and coil outlet temperature at different locations have been compared with the measurements, showing a very good agreement in both modes of operation of the circuit. The validated model helped in the interpretation of the experimental results, such as the backflow at the coil inlet -which cannot be measured- or the non-monotonic outlet temperature evolution following the current dump. Furthermore, the code was used to qualify the isochoric method for the quantification of the deposited energy due to AC losses, as it was the only method applicable in case of current dumps from high current.**

***Index Terms*—Central Solenoid Module, ITER, thermal-hydraulic, validation.**

I. Introduction

THE ITER Central Solenoid Modules (CSMs) are being manufactured and tested at General Atomics, Poway (CA), US [1]. The tests of the first three modules were completed in 2020–2022 [2], [3] and one of the aims of the test campaigns was the quantification of AC losses [4], [5]. Each module is wound using double-pancakes (DP) made of Nb_3Sn Cable-in-Conduit Conductors, cooled with forced-flow supercritical helium at 4.5 K. The coil was equipped with temperature sensors as well as flow meters and pressure sensors which were used to estimate the energy deposited due to AC losses, adopting both calorimetric and isochoric methods [4]. The test campaign was also a unique opportunity to validate thermal-hydraulic codes, such as the 4C code [6], to assess their reliability to reproduce key transients in full-scale coils.

Manuscript received 13 November 2022; revised 17 March 2023 and 23 March 2023; accepted 23 March 2023. Date of publication 30 March 2023; date of current version 10 April 2023. The work was financially funded by UT-Battelle under Grant #534/2016. *(Corresponding author: Andrea Zappatore.)*

A. Zappatore, R. Bonifetto, and R. Zanino are with the NEMO group, Dipartimento Energia, Politecnico di Torino, 10129 Torino, Italy (e-mail: andrea.zappatore@polito.it; roberto.bonifetto@polito.it; roberto.zanino@polito.it).

N. Martovetsky is with the Lawrence Livermore National Laboratory, Oak Ridge National Laboratory, Oak Ridge, TN 37830 USA (e-mail: martovetskyn@ornl.gov).

Color versions of one or more figures in this article are available at https://doi.org/10.1109/TASC.2023.3263136.

Digital Object Identifier 10.1109/TASC.2023.3263136

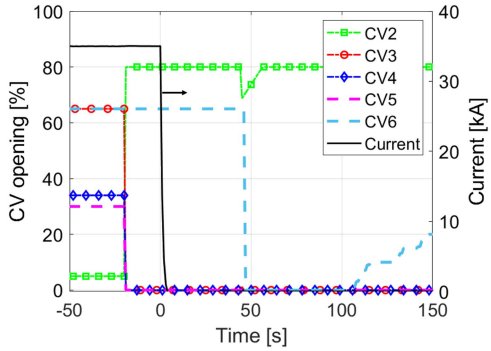

Fig. 1. Evolution of the valve opening before and after a 35 kA current dump. Time 0 s is set at the current dump start.

In this work, the validation of the 4C thermal-hydraulic model adopted to simulate the fast current discharge tests in CSM1 is presented. The paper is organized as follows: the experimental setup and the available diagnostics are first described; then a brief description of the 4C model is presented and finally the validation results in two different operating conditions are discussed.

II. Experimental Setup and Diagnostics

The CSM1 was equipped with temperature sensors on the pipe at each DP outlet. Only three DP inlet pipes were equipped with thermometers. On those pipes, mass flow meters and pressure sensors were also present. The CSM1 common inlet and outlet pipes were both equipped with thermometers and pressure sensors, see the schematics of the model in Section III below.

The AC losses were induced through current dumps from different initial levels. Current dumps from 5, 10, 15, 20, 22.5, 30, 35 and 40 kA were performed. After the current dump was triggered, the current decreased exponentially with a time constant around 6.5 s, depending on the heating up of the resistor bank. During the current dump, both coupling and hysteresis losses are generated due to the coil self-field variation. The heat deposited led to an increase in the pressure and temperature of the helium, which was measured by the set of sensors described above.

In case of dumps from a current level larger than 25 kA, the coil was bypassed in order to protect the cold circulator from the backflow due to the large heat deposition in the coil. The procedure started with the closure of the control valves (CV) on the return lines (CV3-5 in Fig. 1), while a bypass valve was

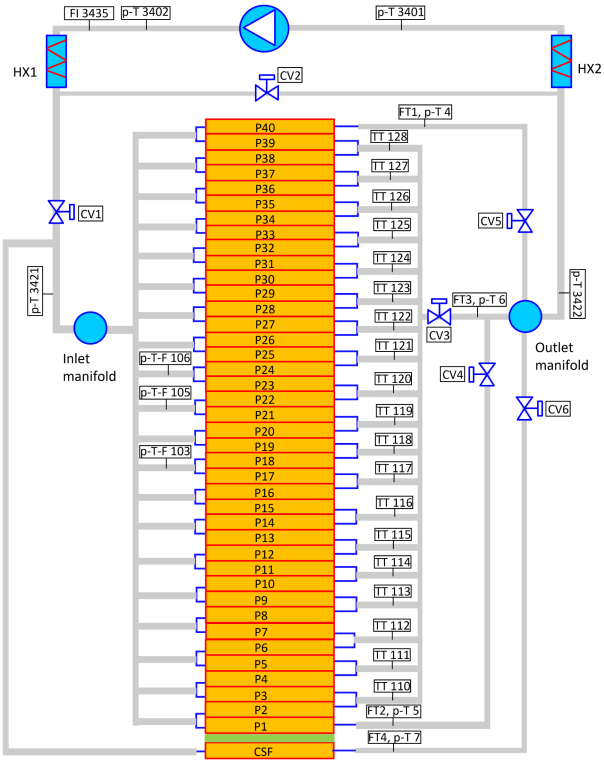

Fig. 2. Cryogenic circuit model with control and bypass valves (CVs) of the CSM cooling loop. The available thermal-hydraulic sensors (p = pressure, T = temperature and F or FT = mass flow rate) are also shown.

opened (CV2 in Fig. 1). The Coil Supporting Frame (CSF) on which the coil was placed was also bypassed closing CV6. After this, the current was dumped and after several seconds the valves were slowly brought back to their nominal state, to cool the helium which was trapped into the CSM1 and CSF hydraulic channels.

III. 4C Model of the CSM1

The model of the CSM1 implemented in the 4C code is reported in Fig. 2.

The winding pack (WP) includes the 1D model of each hydraulic channel. The model solves the heat equation in the jacket and in the cable as well as a set of Euler-like equations for the speed, pressure and temperature of the helium. The heat transfer between adjacent turns and pancakes is taken into account modelling the inter-turn/inter-pancake insulation as a lumped thermal resistance. The heat transfer was calibrated on the CSM Mock-up experiment and it has been cross-checked on the CSM1 itself, see [7].

The CSF is modelled as an hydraulic channel constituted only by the jacket, whose length is that of the cooling pipe of the CSF (37.5 m), while its cross-section is such that the total solid mass of the CSF is preserved. The heat transfer between the CSM and the CSF is modelled as the inter-pancake one, considering that the insulation layer is 8 mm thick.

The cryogenic circuit of the CSM and CSF is modelled using a 0D/1D approach. It includes the cold circulator, which

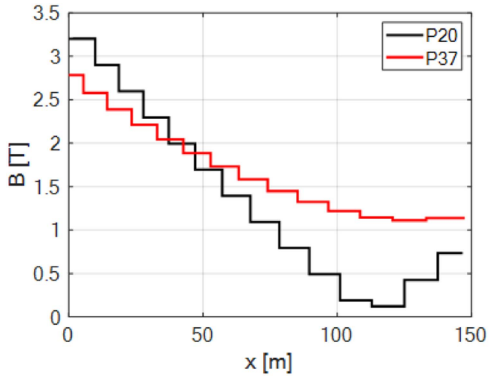

Fig. 3. Distribution of the magnetic field adopted in the simulation in P20 and P37 when the current is 15 kA.

is modelled as a 0D object, whose nominal characteristic is implemented in the code. Two heat exchangers are included and they are modelled as 1D pipes in contact with a perfect heat sink at 4.5 K, accounting also for the pressure drop in these elements. All the control and bypass valves are considered, see Fig. 2, and they are modelled assuming a linear characteristic. In addition, the inlet and outlet manifolds are modelled as 0D volumes. Note that other clients of the cryogenic circuit, such as the current leads, are not taken into account in the model as they play a minor role in the dynamics of the phenomenon under analysis. The operation point of the cold circulator is tuned in order to match the experimental total mass flow rate, considering that the He flowing in the other clients is not modelled here. The circuit model provides consistent boundary conditions to the WP and vice versa at each time step. Further details about the modelling approach and the architecture of the syncronization as well as of the exchange of information between the WP and circuit modules of the code can be found in [6]. The evolution of the opening of the valves during the transient is input to the model from that recorded during the experiment, see again Fig. 1.

The AC losses are modelled using analytical formulae [8] taking into account both hysteresis and coupling losses as follows:

$$P_{coup} = \frac{n\tau}{\mu_0} \cdot \left(\frac{dB}{dt}\right)^2 \cdot A_{sc} \tag{1}$$

$$P_{hyst} = \frac{2}{3\pi} \cdot J_C \cdot d_{eff} \cdot \left|\frac{dB}{dt}\right| \cdot A_{sc} \tag{2}$$

where $n\tau$ is the single time constant (here assumed equal to 570 ms, that corresponds to that of the virgin conductor [9]), μ_0 is the permeability of the vacuum, B is the magnetic field at a given axial location of each hydraulic channel, see, e.g., the distribution along two different channels when the coil is charged at 15 kA in Fig. 3, A_{sc} is the cross-section of the superconducting strands, J_C is the critical current density, d_{eff} the effective diameter of the superconducting strands (here assumed equal to 29 μm [10]).

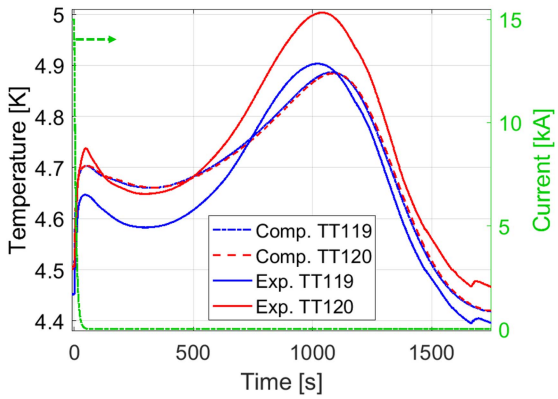

Fig. 4. Dump from 15 kA: comparison between measured and computed coil outlet temperature at half the height of the coil (outlet of DP20-21 and DP22-23). Time 0 s is set at the current dump start. The evolution of the current is also shown.

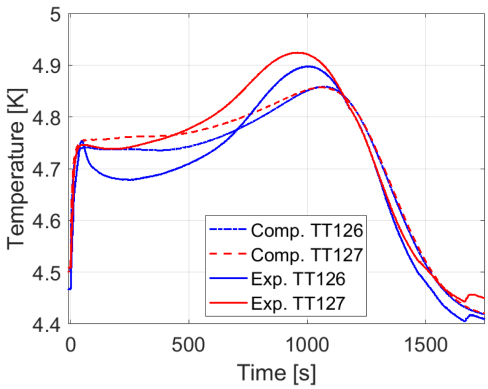

Fig. 5. Dump from 15 kA: comparison between measured and computed coil outlet temperature at the top of the coil (outlet of DP34-35 and DP36-37). Time 0 s is set at the current dump start.

IV. Validation Results

All the current dumps specified in Section II have been simulated, except for those at 5 kA because they produced a very small (<0.05 K) temperature increase due to the small energy deposition, thus they are not interesting for the purpose of the work, i.e., the validation of the CSM model implemented in the 4C code.

The relevant quantities for the validation are the local and global mass flow rate, the temperature measured at different locations and the pressure in the circuit. For brevity, only some of the results for the 15 kA and for the 35 kA dump are shown here, for the low and high current case, respectively. A very similar qualitative picture and quantitative agreement for all the other current dumps was obtained.

A. Low Current

The comparison of the computed and measured evolution of the temperature is reported in Figs. 4 and 5. The evolution of the temperature at the outlet of the coil shows a first peak right after the current dump and a second peak after about a transit time

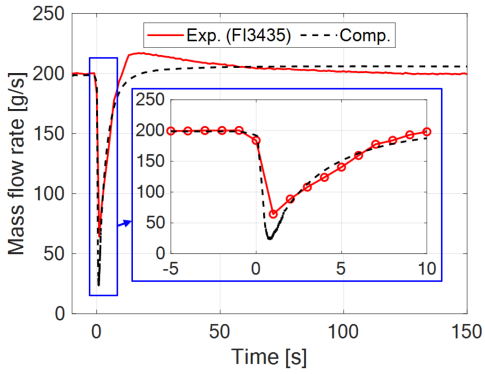

Fig. 6. Dump from 15 kA: comparison between measured and computed mass flow rate in the coil main supply line. Time 0 s is set at the current dump start. A zoom where there is the minimum of the mass flow rate is also shown.

of the He inside the coil (≃1000 s). This is justified by the fact that the power deposition is spatially non-uniform along each pancake. This, in turn, is a direct consequence of the magnetic field distribution, see Fig. 3, which has its maximum at the coil inner radius, where the He inlets are located, and the minimum is found few turns before the He outlet.

The evolution of the outlet temperature at the top of the coil (Fig. 5) confirms that the two peaks are caused by the distribution of the power deposition in the coil. Indeed, Fig. 5 shows a less evident temperature decrease after the first peak (around t = 300 s) than in the middle of the coil, see again Fig. 4. This is caused by the flatter magnetic field distribution in the top pancakes (see, e.g., P37 compared with the central P20 in Fig. 3), which in turn leads to a flatter distribution of the deposited power.

The outlet temperature at the middle of the coil as well as at the top of the coil are qualitatively reproduced by the numerical model. The difference between the two sensors (both in Figs. 4 and 5) is a constant shift of the order of 0.02 K; indeed it was present even before the dump. On the other hand, the computed values are almost identical, as expected, since there are no thermal drivers (both in the model and in the experiment) that would lead to a difference between the DP outlet temperatures.

The evolution of the total mass flow rate is shown in Fig. 6. Right after the current dump, the large power deposition causes a strong pressurization of the coil. This perturbation travels at the speed of sound in the helium of the circuit (220 m/s at 4 bar, 4.5 K), therefore, in ≃1 s a decrease in the total mass flow rate due to the change in the working point of the circulator is induced. Both the decrease and increase back to the nominal value of the total computed mass flow rate agree very well with the experimental signal. Note, however, that the decrease in the mass flow rate was so fast (in the simulation the minimum is reached ≃1 s after the dump) that the values recorded by the data acquisition system were just a few, see the inset in Fig. 6; therefore the minimum value of the mass flow rate could not be accurately measured due to the low frequency of acquisition (1 Hz). The numerical model computes a lower minimum value of the mass flow rate and a smoother overshoot when the mass flow rate recovers to its nominal value. These differences are, however, localized in time, i.e. they last for few seconds. The

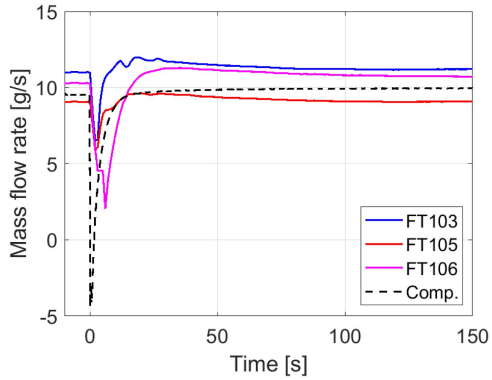

Fig. 7. Dump from 15 kA: comparison between measured and computed mass flow rate at selected DP inlets, where measurements are available. Time 0 s is set at the current dump start.

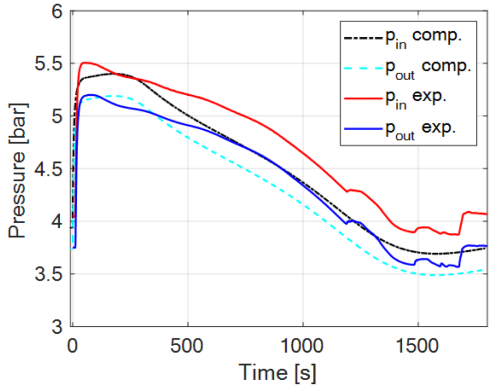

Fig. 8. Dump from 15 kA: comparison of the measured and computed pressure evolution at the coil inlet and outlet. Time 0 s is set at the current dump start.

mass flow rate behavior is, indeed, well reproduced throughout the transient.

The measured and computed local mass flow rate at selected inlet pipes are also in good agreement, see Fig. 7. Locally, at the inlet, the model results showed that backflow was present for few seconds, which could of course not be measured by the Venturi mass flow meters. It is worth highlighting that there is backflow close to the DP inlets even for a current dump from 15 kA, thus with a small power deposition. However, this is due also to the shape of the power deposition, as discussed before, which is higher where the magnetic field is higher, thus close to the inlet. Indeed, the backflow is much less pronounced (<-1 g/s) at the top DP inlets. Note that the computed mass flow rate evolution in the central pancakes is very similar, thus only one computed curve has been reported in Fig. 7.

The comparison of the evolution of the measured and computed pressure is reported in Fig. 8. The computed pressure evolution, both at the coil inlet and outlet, is in good agreement with the measured data. The maximum error is found towards the end of the transient, which is not of much interest here, and it is anyway below 0.25 bar. The most interesting frame of the pressure evolution is at the beginning of the transient, when basically all the power is deposited (in the first $\simeq$25 s after the dump, 95% of the power is deposited). The interest for this portion of the transient is due to the fact that the

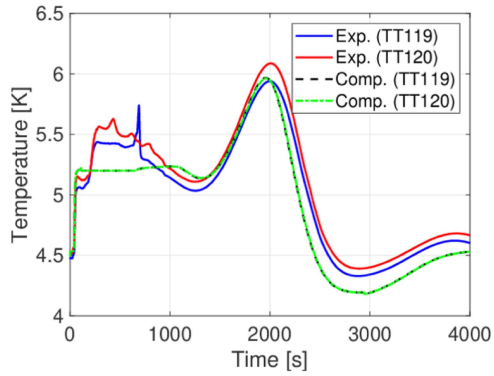

Fig. 9. Dump from 35 kA: comparison between measured and computed coil outlet temperature at half the height of the coil (outlet of DP20-21 and DP22-23). Time 0 s is set at the current dump start.

pressure increase is directly related to the power deposited. Indeed, assuming a constant He volume during the transient, an estimation of the energy deposited can be performed using an isochoric approximation from the initial state (low pressure, before the dump) and the final state (high pressure, when roughly all the power is deposited) [4].

B. High Current

The comparison of the computed and measured outlet temperature at the middle of the coil is reported in Fig. 9 for the dump from high current level, where the valves are operated as described in Section II. The same behavior is obtained at the top of the coil (not shown here for brevity). What happens before the re-opening of the isolation valves, i.e., at t $\simeq$ 1000 s is not of interest, since there was no flow through the pipe on which the thermometer is installed. After that, the flow is restored and the agreement between measured and computed temperature is very good in both the peak, directly connected to the power deposited in the coil, and the decrease of the outlet temperature, driven by the effectiveness of the re-washing of the coil since fresh He started entering the coil. Note that the peaked evolution of the outlet temperature is caused by the non-uniformity of the power deposition, as discussed already in Section IV-A. In this case, however, the peak is observed $\simeq$2000 s after the current dump. This is caused by the isolation of the coil that lasted for $\simeq$1000 s.

In Fig. 10, the comparison of the measured inlet and outlet pressure with those computed is reported. The pressure rise, which is a direct consequence of the energy deposition due to AC losses, is well captured, within 0.3 bar (10.65 bar computed, 10.9 bar measured). Note that the starting pressure of the cryogenic circuit before the dump is 0.2 bar lower in the computation, therefore the pressure jump is very well reproduced, both in amplitude and rate of increase. On the other hand, the initial pressure decrease, due to the gradual opening of CV6 (on the return line of the CSF) from t = 105 s to t = 460 s, is not evident in the simulations as in the experiment. The reproduction of this detail is probably due to the actual cooling path of the CSF as well as its 3D shape, which cannot be modelled in detail with a 1D tool. Nevertheless, the key aspects of the transient, i.e., the fast pressure rise and the coil washing, are captured.

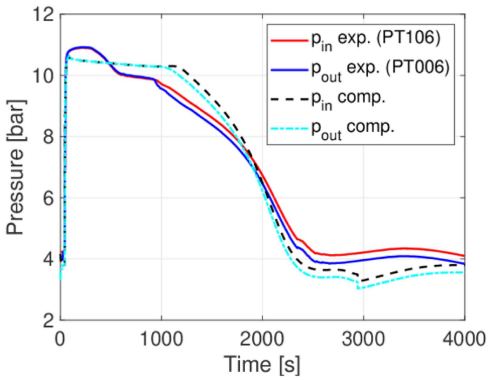

Fig. 10. Dump from 35 kA: comparison of the measured and computed pressure evolution at the coil inlet and outlet. Time 0 s is set at the current dump start.

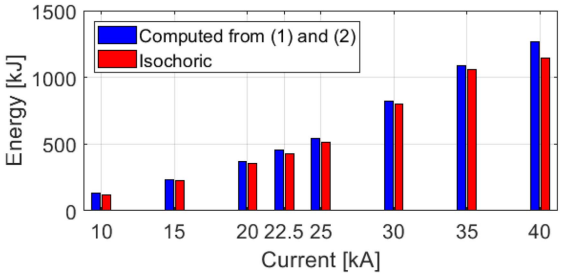

Fig. 11. Comparison of the computed energy deposited by AC losses according to the model described in Section III and the isochoric method applied to the computed results.

A direct application of the validated model is shown in Fig. 11 and discussed hereafter. The isochoric method was chosen as alternative to the calorimetry to assess the losses in case the coil was isolated from the circulator, as discussed in [4]. The accuracy of the isochoric method was not known, therefore it was applied to the numerical results computed with the validated model. The deposited energy assessed with the isochoric method was then compared to the exact deposited energy, computed in the model according to (1) and (2). The comparison is shown in Fig. 11: the validated model helped in the interpretation of the experiment, assessing that the isochoric method provides a very good estimate of the energy deposited by AC losses, (always) underestimating it by 10% at most.

V. Conclusion and Perspective

The 4C code has been validated for the first time against data from a full-scale ITER magnet. The code has been used to simulate the CSM1 current dumps also in case the coil was isolated from the cold circulator through operation of the control valves. The agreement between the measured and computed results in terms of coil outlet temperature, total and local mass flow rates and pressure evolution throughout the current dump and recooling is very good. For all the dumps, the isochoric method shows a satisfactory assessment of the energy deposited (within 10%). The 4 C code is therefore qualified as a reliable tool for the future analyses of ITER magnet operation.

Acknowledgment

The authors would like to thank the GA team for their kind hospitality during the CSM Mock-Up and CSM1 tests.

References

[1] K. Schaubel, A. Langhorn, S. Lloyd, Z. Piec, E. Salazar, and J. Smith, "The ITER central solenoid module final test facility," *Fusion Eng. Des.*, vol. 124, pp. 59–63, 2017. [Online]. Available: https://www.sciencedirect.com/science/article/pii/S0920379617305458

[2] N. Martovetsky et al., "First ITER CS module test results," *Fusion Eng. Des.*, vol. 164, 2021, Art. no. 112169. [Online]. Available: https://www.sciencedirect.com/science/article/pii/S0920379620307171

[3] N. Martovetsky et al., "Testing of the ITER central solenoid modules," *IEEE Plasma Sci.*, vol. 50, no. 11, pp. 4292–4297, Nov. 2022.

[4] M. Breschi et al., "AC losses in the first ITER CS module tests: Experimental results and comparison to analytical models," *IEEE Trans. Appl. Supercond.*, vol. 31, no. 5, Aug. 2021, Art. no. 5900905.

[5] M. Breschi et al., "AC losses in the second module of the ITER central solenoid," *IEEE Trans. Appl. Supercond.*, vol. 32, no. 6, Sep. 2022, Art. no. 4700505.

[6] L. Savoldi Richard, F. Casella, B. Fiori, and R. Zanino, "The 4C code for the cryogenic circuit conductor and coil modeling in ITER," *Cryogenics*, vol. 50, no. 3, pp. 167–176, 2010. [Online]. Available: https://www.sciencedirect.com/science/article/pii/S0011227509001118

[7] A. Zappatore, R. Bonifetto, N. Martovetsky, and R. Zanino, "Development and validation of the 4C thermal–hydraulic model of the ITER Central Solenoid modules," *Cryogenics*, vol. 127, 2022, Art. no. 103552. [Online]. Available: https://www.sciencedirect.com/science/article/pii/S0011227522001345

[8] M. Wilson, *Superconducting Magnets*. London, U.K.:Oxford Univ. Press, 1992.

[9] M. Breschi et al., "Analysis of AC losses in the ITER central solenoid insert coil," *IEEE Trans. Appl. Supercond.*, vol. 27, no. 4, Jun. 2017, Art. no. 4200605.

[10] R. Bonifetto et al., "Modeling the ITER CS AC losses based on the CS insert analysis," *IEEE Trans. Appl. Supercond.*, vol. 29, no. 5, Aug. 2019, Art. no. 4200907.

Open Access funding provided by 'Politecnico di Torino' within the CRUI CARE Agreement